Scramjet Inlets

Professor Michael K. Smart
Chair of Hypersonic Propulsion
Centre for Hypersonics
The University of Queensland
Brisbane 4072
AUSTRALIA

m.smart@uq.edu.au

ABSTRACT

The supersonic combustion ramjet, or scramjet, is the engine cycle most suitable for sustained hypersonic flight in the atmosphere. This article describes some challenges in the design of the inlet or intake of these hypersonic air-breathing engines. Scramjet inlets are a critical component and their design has important effects on the overall performance of the engine. The role of the inlet is first described, followed by a description of inlet types and some past examples. Recommendations on the level of compression needed in scramjets are then made, followed by a design example of a three-dimensional scramjet inlet for use in an access-to-space system that must operate between Mach 6 and 12.

NOMENCLATURE

A	area (m^2)	x	axial distance (m)
C_f	skin friction coefficient	ϕ	equivalence ratio
D	diameter (m); Drag (N)	ϑ	constant in mixing curve
f_{st}	stoichiometric ratio	η_c	combustion efficiency
F	stream thrust (N)	η_{KE}	kinetic energy efficiency
F_{add}	additive drag (N)	η_{KE_AD} adiabatic	kinetic energy efficiency
F_{un}	uninstalled thrust (N)	η_o	overall scramjet efficiency
h	enthalpy (289K basis) (J/kg)	η_n	nozzle efficiency
h_{pr}	heat of combustion (J/kg of fuel)		
H_t	total enthalpy (298K basis) (J/kg)	**Subscript**	
L	length (m)	c	cowl
m_c	mass capture ratio	comb	combustor
$\dot{m}$	mass flow rate (kg/s)	f	fuel
M	Mach number	in	inflow
P	pressure (Pa)	out	outflow
Q	heat loss (kJ)	isol	isolator
q	dynamic pressure (Pa)	n,N	nozzle
T	temperature (K); thrust (N)	SEP	separation
u,V	velocity (m/s)		

1.0   INTRODUCTION

The desire for hypersonic flight within the atmosphere has motivated multiple generations of aerodynamicists, scientists and engineers. In the late 1950's and early 1960's it became clear that while rocket propulsion had the potential for access-to-space and the ability to reach many parts of the globe on ballistic trajectories, only an airbreathing propulsion system could facilitate practical hypersonic flight. Antonio Ferri[1] aptly described the important differences between rockets and airbreathing engines as:

1) The potential specific impulse of airbreathing propulsion is much larger than any chemical rocket, due to the fact it carries only fuel and not oxidiser.

2) Structural weight of an airbreathing engine is larger for the same thrust than a rocket, because it must process air (oxygen and nitrogen) and have an intake, whereas the rocket has an oxidiser tank and pressurization system.

3) The thrust of an airbreathing engine is a function of flight Mach number and altitude. Large thrust per unit frontal area can only be obtained in the dense atmosphere, while rockets can operate at high thrust per unit frontal area in a vacuum.

4) The necessity for flight in the atmosphere introduces severe structural problems for the airbreathing engine associated with aerodynamic heating and vehicle drag. However, the vehicle has a greater potential for manoeuvring than a rocket traveling in a vacuum, through the use of aerodynamic lift.

It was recognized at the time that a hypersonic airbreathing propulsion system could fulfill many roles that a rocket could not, including hypersonic cruise and recoverable space launchers.

The airbreathing engine cycle best suited to hypersonic flight is the supersonic combustion ramjet, or scramjet. This type of engine can be properly viewed as an extension of the very successful ramjet engine cycle, which uses shock wave compression in the inlet in lieu of the compressor in a gas-turbine engine. In a ramjet, air entering the combustor is first decelerated to subsonic speeds, where fuel is injected and burnt, and finally expanded through a second throat to a thrust nozzle. As flight speeds increase above Mach 5, reducing the air to subsonic conditions produces two problems; (1) significantly increased shock losses in the inlet, particularly at the terminal normal shock, and (2) significantly increased flow temperatures in the combustor. The second of these problems not only creates material/structural issues in the combustor, but also leads to chemical dissociation in the nozzle expansion and a consequent energy loss from the engine cycle.

The flight corridor for scramjet propelled vehicles, either for cruise or ascent to low-earth-orbit, is constrained at upper altitude by the need to operate the airbreathing engine, and at lower altitude by structural limits of the vehicle. Figure 1 gives an indication of these limits, and includes a suggested ascent trajectory for an airbreathing access-to-space vehicle, with turbojet operation up to Mach 3-4, scramjet operation up to Mach 15-17 and then rocket based propulsion for the final boost to low earth orbital velocity, which is approximately 7.9 km/s.

This article is concerned primarily with the design of the compression system for scramjet engines. Efficient combustion of fuel requires that supersonic airflow be supplied to the combustor at a suitable pressure, temperature and mass flow rate. For a scramjet traveling at speeds greater than Mach 5 and at altitudes in the flight corridor of Fig. 1, this requires significant compression and heating of the air. For an airframe-integrated scramjet, both the vehicle forebody and inlet share this task. A multitude of different forebody/inlet configurations have been developed by many researchers[2], each designed to generate a specified level of compression over a range of flight Mach numbers. The performance of such compression systems can be separated into two key parameters; (1) capability, or how much compression is performed, and (2) efficiency, or what level of flow losses does the forebody/inlet generate during the

compression process. Meaningful discussions of inlet performance must include both parameters as, for example, a highly efficient inlet can be very easily designed if it is required to do little compression.
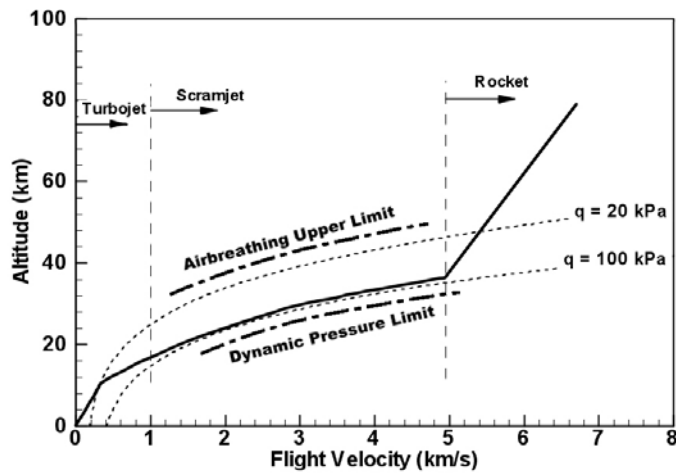

Figure 1: Hypersonic airbreathing flight corridor.

Figure 2 shows a schematic of the internal flowpath of an airframe-integrated scramjet with particular reference stations highlighted. In keeping with the convention of Heiser & Pratt[3], station 0 is in the freestream flow ahead of the vehicle, and a streamtube with area A_0 captures the airflow processed by the engine. Station 1 is downstream of the vehicle forebody shock and represents the properties of the flow that enters the inlet. Station 2 is at the inlet throat, which is usually the minimum area of the flowpath, and the length between stations 2 and 3 is referred to as the isolator. Station 3 represents the start of the combustor (where fuel is added), and fuel and air is mixed and burned by the end of the combustor at station 4. The nozzle includes an internal expansion up to station 9, and an external expansion to station 10 at the end of the vehicle.
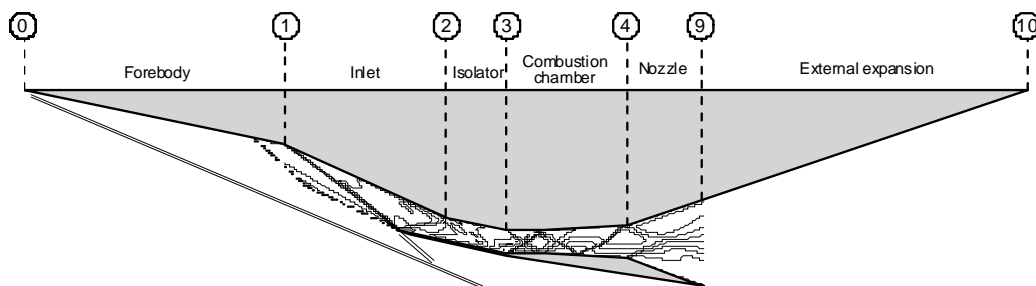
Figure 2: Flow stations in a scramjet engine.

Performance analysis of scramjet inlets involves the determination of the flow conditions at the inlet throat (station 2 of Fig. 2). A common parameter used to quantify the efficiency of the forebody/inlet compression is the kinetic energy efficiency, η_{KE}. The usefulness of this parameter, compared to many others, is that it can be used for non-ideal gas processes, and that its value has been found to be relatively

independent of flight Mach number for a particular class of inlets. The definition of η_{KE} is the ratio of the kinetic energy the compressed flow would achieve if it were expanded isentropically to freestream pressure, relative to the kinetic energy of the freestream, and is most easily described on a Mollier diagram (Fig. 3). Here the flow entering the engine is compressed from p_0 to p_2. During the compression there is heat loss to the forebody/inlet structure, and:

$$\eta_{KE} = \frac{1/2 u'^2_2}{1/2 u_0^2} = \frac{H_{t2} - h'_2}{H_{t0} - h_0} \tag{1}$$
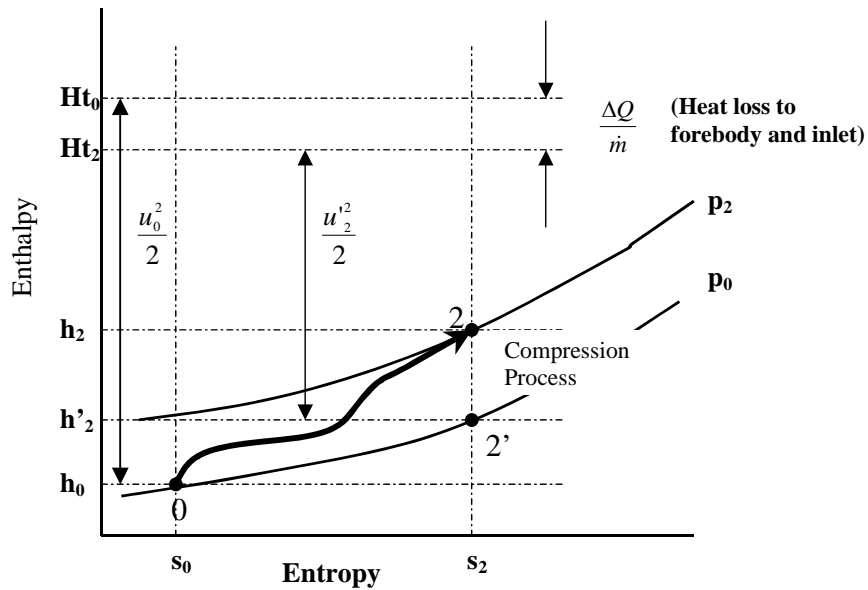
Figure 3: Mollier diagram of inlet compression process.

In some instances the adiabatic kinetic efficiency, η_{KE_ad} is used. This parameter does not account for heat loss to the structure, and is defined as:

$$\eta_{KE,ad} = \frac{H_{t0} - h'_2}{H_{t0} - h_0} \tag{2}$$

When conducting scramjet performance calculations, two common methods for determining the properties at the inlet throat are; (1) use an empirical relation for η_{KE} or η_{KE_AD} in combination with a capability parameter, and (2) use CFD to perform a numerical simulation of the forebody/inlet flowfield. An empirical correlation for η_{KE_ad} developed by Waltrup[4] in terms of the ratio of throat Mach number to freestream Mach number, M_2/M_0, is as follows:

$$\eta_{KE\_AD} = 1 - 0.4 \left\{ 1 - \frac{M_2}{M_0} \right\}^4 \tag{3}$$

This expression relates inlet efficiency to an inlet capability parameter, M_2/M_0, so it satisfies the requirement for being a useful relation. Figure 4 compares eqn. 3 against experimental data and computational solutions for a range of inlet geometries at hypersonic conditions. Based on Fig. 4 it

appears that for higher compression level inlets, eqn. 3 is conservative. For $M_2/M_0 < 0.5$ the current author uses the empirical fit also shown in Fig.4.
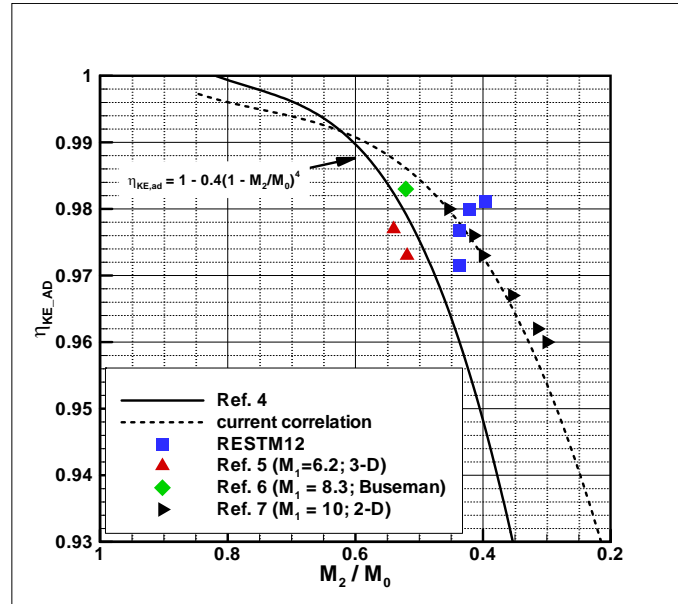

$$\eta_{KE,ad} = 1 - 0.4(1 - M_2/M_0)^4$$

Figure 4: Inlet efficiency data compared to a number of correlations.

This article first describes the general types of inlets that are applicable to hypersonic flight. Next some example systems are described and commented upon. A key question in any scramjet design is "how much compression should a scramjet inlet do?" This issue is examined and some recommendations made. Finally, a test case involving the design of a 3-D inlet for a scramjet based access-to-space vehicle is described.

2.0 SCRAMJET INLET TYPES AND EXAMPLES

Hypersonic inlets used in scramjets fall into three-different categories, based on the type of compression that is utilized. These three types are (i) external compression, (ii) mixed compression and (iii) internal compression. A schematic of an external compression inlet is shown in Fig. 5. Here, as the name suggests, all the compression is performed by flow turning in one direction by shock waves that are external to the engine. These inlet configurations have large cowl drag, as the flow entering the combustor is at a large angle relative to the freestream flow, however, external compression inlets are self-starting and spill flow when operated below the design Mach number (this is a desirable feature for inlets that must operate over a large Mach number range). A schematic of a mixed compression inlet is shown in Fig. 6. Here the compression is performed by shocks both external and internal to the engine, and the angle of the external cowl relative to the freestream can be made very small to minimize external drag. These inlets are typically longer than external compression configurations, but also spill flow when operated below the design Mach number. Depending on the amount of internal compression, however, mixed compression inlets may need variable geometry in order to start. A schematic of an internal compression inlet is shown in Fig. 7. Here all the compression is performed by shock waves that are internal to the engine. This type of inlet can be shorter than a mixed compression inlet, but it does not allow easy integration with a vehicle. It maintains full capture at Mach numbers lower than the design point, but its most significant limitation is that extensive variable geometry is always required for it to start.
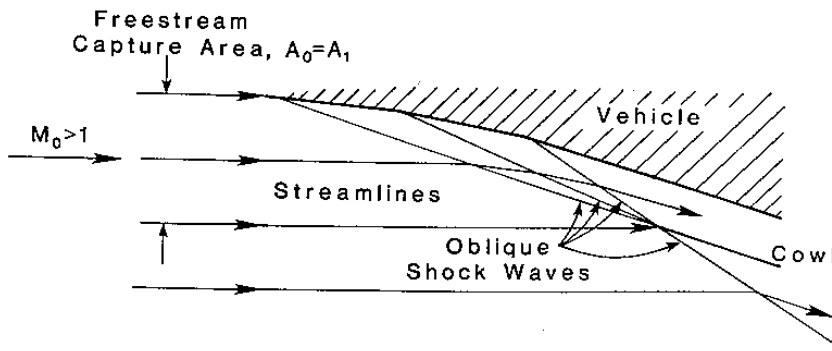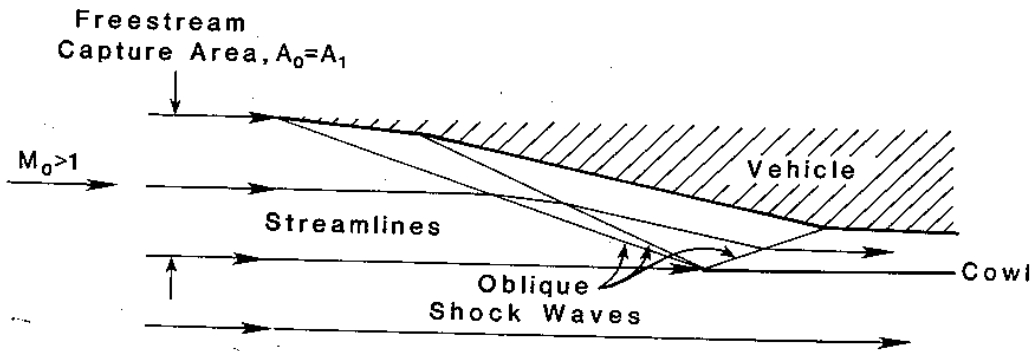
Figure 5: External compression inlet (Heiser and Pratt[3]).

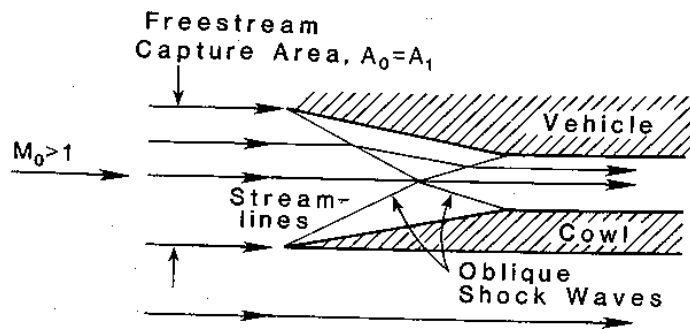**Figure 6: Mixed external and internal compression inlet (Heiser and Pratt[3]).**

Figure 7: Internal compression inlet (Heiser and Pratt[3]).

Figure 8 shows a number of inlet configurations that have been developed as part of scramjet engine research since the 1960's. The pod-type Hypersonic Research Engine (NASA Langley 1964-70 – Ref. 8) included an axisymmetric translating-spike inlet leading to an annular combustor. It was designed for Mach 5-7 operation and has a clear connection to gas-turbine heritage. The external drag of this configuration was found to be too high to generate positive net thrust. The sidewall compression inlet configuration (NASA Langley 1975-85; Ref. 9) was designed to integrate smoothly with a hypersonic vehicle as a series of modular ducts. It had a fixed geometry (self-starting), mixed compression inlet.

Numerous incarnations of this inlet have been tested by many groups. The SCRAM missile configuration (APL 1965-85; Ref. 10) had multiple 3-D streamline traced inlets designed to operate with fixed geometry between Mach 3-8. Another missile configuration, known as the Dual Combustion Ramjet (APL 1975-95; Ref. 11), was an axisymmetric engine that included multiple subsonic and supersonic inlets designed to operate between Mach 3-8. Here the subsonic inlets were used to supply very hot gas to a fuel ignition region, while the mixed compression supersonic inlets operated in the conventional way. The inlet on the Hyper-X vehicle was a 2-D mixed compression inlet (NASA Langley 1996-2004; Ref. 12) that was a legacy configuration from the NASP Program. It included a rotating door to enable the inlet to start and also to allow close-off.
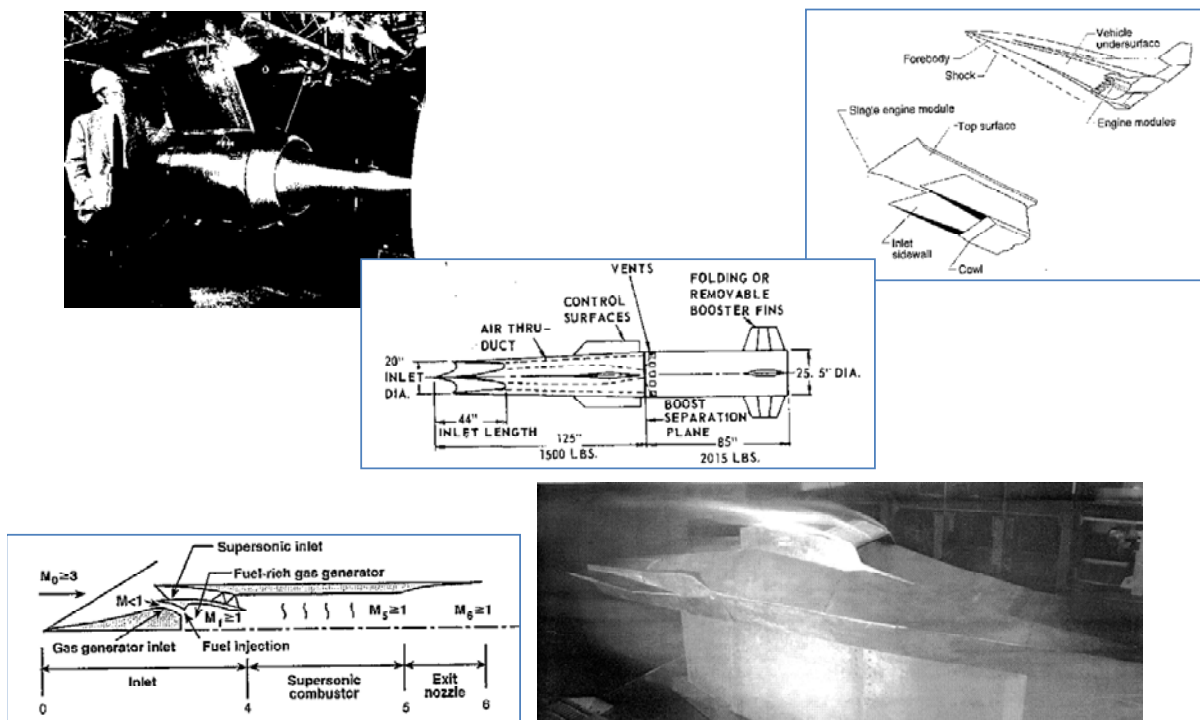
Figure 8: Scramjet configurations.

There are some key observations that can be made about all these configurations:

1) All have mixed compression inlets.

2) All were designed to operate over a range of Mach number.

3) Only the HRE and Hyper-X inlets involved variable geometry.

It is also clear that the geometry and operation of the inlet was a dominating feature of the overall scramjet configuration.

3.0 COMPRESSION REQUIREMENTS

A critical question in the design of a scramjet inlet is "how much compression is needed?" Too much compression can place extra system constraints on the inlet such as the need for variable geometry or boundary layer bleed, and can lead to large losses and external drag. Too little compression can make adequate ignition and combustion of fuel very difficult and lead to low cycle efficiency. In practice, the

optimal level of inlet compression for a particular application is dependent on numerous conflicting factors, the most important of which are:

1) Overall scramjet cycle efficiency.

2) Non-equilibrium effects in the nozzle.

3) Need for robust combustion.

4) Operability requirements (inlet starting, boundary layer separation, etc.).

The remainder of this section involves a discussion of these factors.

3.1 Scramjet Cycle Efficiency

The level of compression performed by a scramjet inlet has important effects on the overall cycle efficiency (η_o) of the engine, which is defined as:

$$\eta_o = \frac{F_{un} V_0}{\dot{m}_{air} h_{pr}} \tag{4}$$

where F_{un} is the un-installed thrust, V_0 is the flight velocity, $\dot{m}_{air}$ is the airflow through the engine and h_{pr} is the heat release available from complete combustion of fuel and air (120 MJ/kg for hydrogen). It is therefore instructive to perform a general study of how compression level effects η_o. In the current article this will involve the use of stream thrust based methods for the calculation of scramjet performance first introduce by Curran and Craig[13].

3.1.1 Stream Thrust Based Performance Methods

The performance of a scramjet engine, either uninstalled or when integrated on a hypersonic vehicle, is most easily determined by what is called stream thrust analysis. This technique conserves the fluxes of mass, momentum and energy on strategically placed control volumes to determine the propulsive forces on the vehicle. Figure 9 shows a schematic of a control volume that moves with and surrounds a hypersonic vehicle powered by a scramjet engine. Airflow enters the control volume at the flight conditions, fuel is added to the air in the combustor and the flow exits through the vehicle nozzle. For ease of analysis, the flow exiting the control volume is usually represented by a flux-conserved one-dimensional average of the real non-uniform exhaust plume.
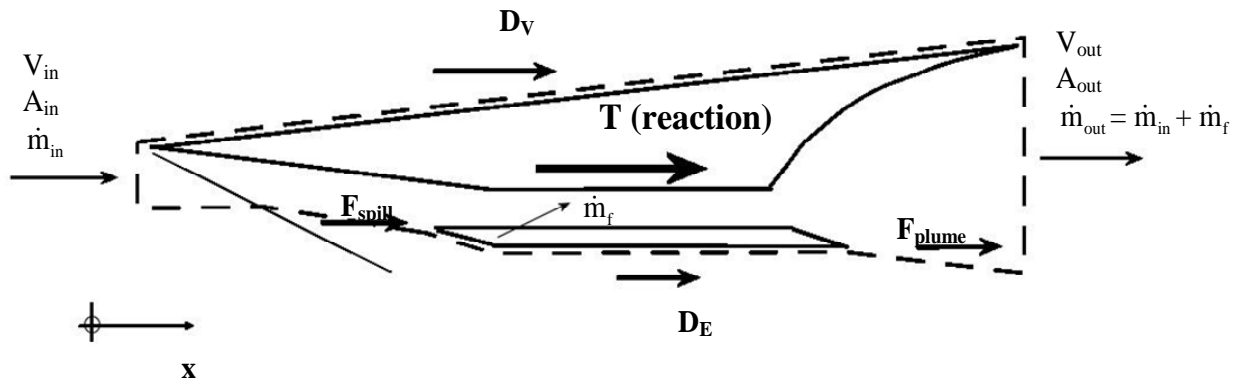

Figure 9: Schematic of control volume used for scramjet performance analysis.

For steady state flow through the control volume of Fig. 9, Newtons 2nd Law can be used to equate the summation of the axial forces on the control volume with the axial momentum flux across its surface, yielding the following relation for the uninstalled thrust of the engine, F_{un},:

$$F_{un} = p_{out} A_{out} + \left(\dot{m}_f + \dot{m}_{in} \right) V_{out} - p_{in} A_{in} - \dot{m}_{in} V_{in} - F_{add} \tag{5}$$

where $T = F_{un} - D_v - D_{ex}$, and the spillage (F_{spill}) and plume (F_{plume}) drag have been combined into a single force called the additive drag (F_{add}). Using the definition of stream thrust, $F = pA + \dot{m}V$, we can express eqn. 5 as:

$$F_{un} = F_{out} - F_{in} - F_{add} \tag{6}$$

Equation 6 indicates that the uninstalled thrust of an engine can be determined with knowledge of the stream thrust of the air entering the engine, the additive drag, and the stream thrust of the flow exiting the engine. The flow enters the engine at ambient conditions and at the flight velocity, so calculation of F_{in} reduces to a determination of the freestream capture area. Air spillage (and therefore spillage drag) decreases as the vehicle speed approaches the design point of the engine, and the plume drag varies depending on the amount of under-expansion in the nozzle. Both these forces are usually estimated through CFD analysis or through rules-of-thumb based on empirical or experimental databases. Determination of F_{out} requires an involved analysis that follows the air through the complete scramjet flowpath.

### 3.1.2 Scramjet Cycle Calculations

To illustrate the effect of compression level, a sample study was performed to calculate overall scramjet efficiency over a range of flight Mach numbers between 6 and 12. The assumptions made in the analysis were as follows:

1) Flight dynamic pressure, q_0 = 50 kPa.

2) Atmospheric static temperature, T_0 = 220 K.

3) Engine mass capture, $\dot{m}_{air}$ = 0.5 kg/s, with no spillage.

4) Negligible additive drag, F_{add} = 0.0 N.

5) No heat loss to the inlet or the nozzle.

6) Gaseous hydrogen fuel at T_f = 300 K (h_{pr} = 120 MJ/kg).

7) Normal fuel injection (no thrust from fuel).

8) Circular combustor with length, L_{comb} = 0.4 m and area ratio, A_4/A_2 = 2.0.

9) Combustor skin friction coefficient, C_f = 0.002.

10) Combustor heat loss calculated using Reynolds analogy and T_{wall} = 500 K.

11) Isolator length, L_{isol} = 0.15 m.

12) Nozzle expansion area ratio, A_{10}/A_0 = 1.5.

At each flight Mach number, F_{un} and η_o were calculated for increasing compression level by separating the engine cycle into three processes;i.e. compression, combustion and expansion as described below.

Compression

A complete definition of the compression process requires both a compression level and an efficiency to be defined. In this study the desired compression level was specified in terms of an inlet temperature ratio, $\psi = T_2/T_0$, and the corresponding efficiency is determined from the η_{KE_ad} curve plotted in Fig. 4. Given these two parameters, the flow properties at the exit of the inlet were determined by accounting for real gas effects through the use of calls to equilibrium air computer routines. Figure 10 shows plots of the η_{KE_AD}, M_2, $P_{rat} = P_2/P_0$ and $A_{rat} = A_0/A_2$ calculated in this way, with a variation of temperature ratio between $\psi = 3$ and 10. For flight at Mach 6, the maximum temperature ratio was limited to $\psi = 5$, as higher temperature ratio led to the throat Mach number approaching sonic. This phenomenon also limited ψ to 7 and 9 for flight at Mach 8 and 10, respectively, while the Mach 12 flight case included the full range of ψ from 3 to 10. The adiabatic kinetic energy efficiency curves in Figure 10(a) show the expected reduction in η_{KE_AD} as ψ increased for all flight Mach numbers, with η_{KE_AD} improving as flight Mach number increased. The throat Mach number, compression ratio and contraction ratio curves plotted in Figs. 10(b) – (d) show a decreasing M_2 with greater ψ, and increasing P_{rat} and A_{rat} with greater ψ. An interesting point to note is that for a given inlet temperature ratio, the compression ratio generated is greatly increased by improved inlet efficiency. Finally, the inlet exit pressure, P_2, is plotted in Fig. 10(e). For inlets that have efficiencies close to the curve used in this study, P_2 can become very high (of the order of 2.5 atmospheres) for the higher ψ values used in this study.
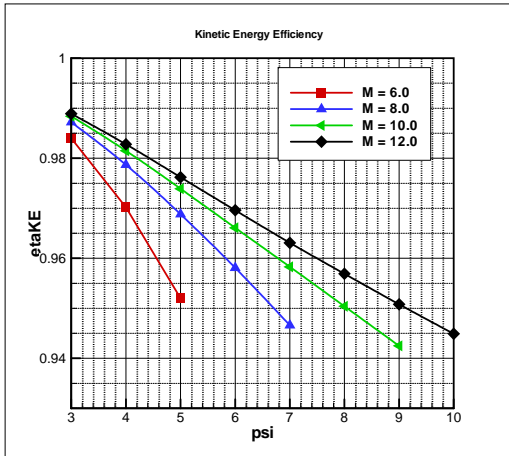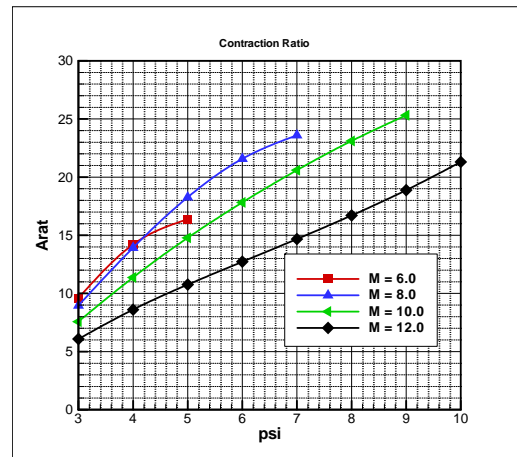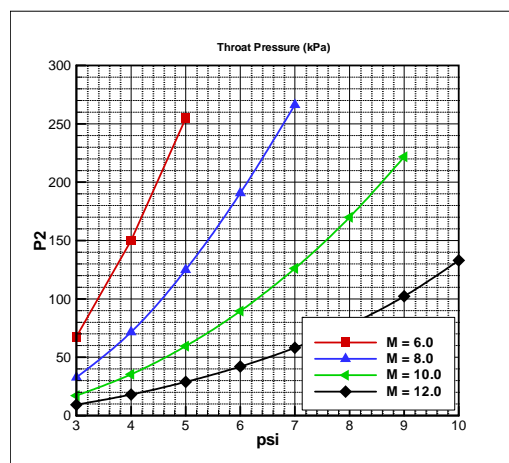
(a)
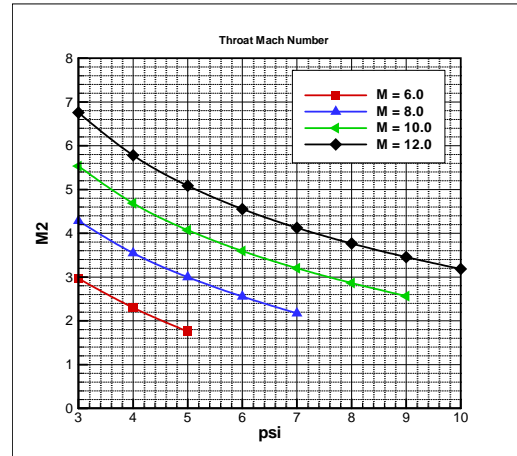
(b)
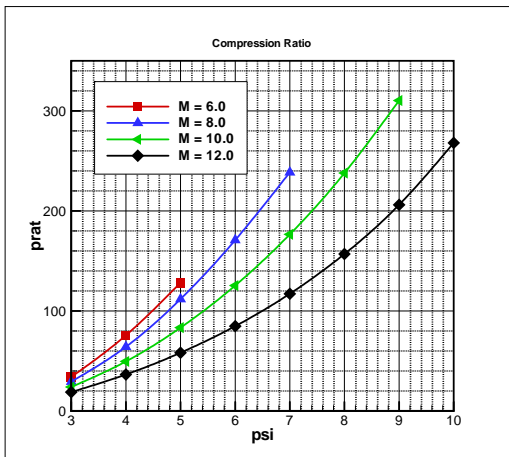
(c)

(d)

(e)

Figure 10: Plots of inlet performance parameters for M = 6-12 and ψ = 3-10.

Combustion

The processes of fuel addition, fuel/air mixing and combustion were modelled in this study using a stream thrust based cycle analysis that conserves mass, momentum and energy with the assumption of quasi-one-dimensional flow. Both pure supersonic combustion and dual-mode combustion (combined subsonic/supersonic) were modelled using the methodology described in Ref. 14. At conditions where the combustion generated pressure rise was such that flow separation occurred, a diffuser model[15] was used to estimate the effects of the shock train that forms upstream of fuel injection. This model enabled engine operability limits to be established, and the maximum fuel level was limited in these instances. The combustor flows of interest were modelled as mixtures of thermally perfect gases that were in thermodynamic equilibrium. Furthermore, the combustion of fuel was assumed to be "mixing limited", meaning that once the fuel was allowed to mix with the air, the mixture immediately went to an equilibrium state of fuel, air and combustion products.

Figure 11 shows a schematic of a scramjet combustor with air entering from the left at station 2, fuel injection at station 3, and combustion products exiting to the right at station 4. The gross parameters for the air entering the combustor are mass flow rate, $\dot{m}_2$, stream thrust, F_2, and total enthalpy, H_{T2}. The incoming flow area is A_2. The gross parameters associated with fuel injection are fuel flow rate, $\dot{m}_f$, fuel stream thrust, F_f, and fuel total enthalpy, H_{Tf}. As the fuel/air mixture travels downstream, a proportion of the fuel is allowed to react with the air, and the gross parameters of the flow are calculated by conserving mass, momentum and energy using a control volume analysis associated with incremental steps of length Δx along the combustor. Through calls to thermodynamic equilibrium routines, state properties and the velocity are determined at all stations along the combustor.
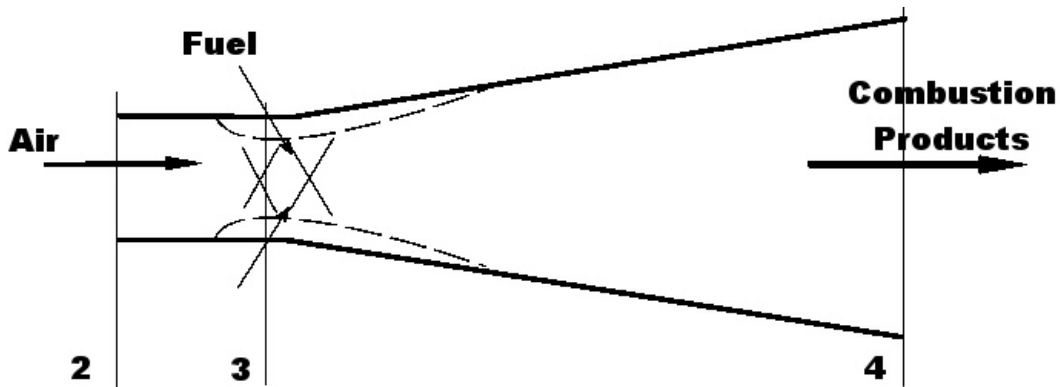

Figure 11: Schematic of the combustor analysis.

In a typical combustor calculation the area distribution of the combustor was specified a priori. The amount of fuel that was allowed to react with the air at a particular station was dictated by a combustion efficiency curve, $\eta_c(X)$, that took the form:

$$\eta_c = \eta_{c,tot}\left[\frac{\vartheta X}{1+(\vartheta-1)X}\right] \qquad (7)$$

where $\eta_{c,tot}$ is the combustion efficiency at the end of the combustor, $X = (x-x3)/(x4-x3)$ and ϑ is an empirical constant of order 1 to 10 which depends on the rate of mixing[3]. For the current study $\eta_{c,tot}$ was set to 0.8 at all times and a value of $\vartheta = 5.0$ was used. These values correspond to robust operation of the engine. The proportion of the fuel that has not mixed with the air was considered to be inert, and was

included as un-reacted species in the thermodynamic equilibrium calls. The incremental area change (ΔA) across a control volume of length Δx is known from the area distribution, and incremental changes to the stream thrust and total enthalpy from fuel combustion, friction forces, pressure forces and heat loss were calculated to determine the stream thrust and total enthalpy of the flow exiting the control volume. The analysis started at station 2, and marched along the combustor until station 4 was reached. Some iteration was required for cases where dual-mode combustion occur[19].

Figure 12 shows example plots of properties through the combustor for the case of $M_0 = 8.0$, $\psi = 6.0$, where x = 0.0 m is at the exit of the inlet (station 2), fuel is injected at the end of the isolator (x = 0.15 m) and the combustor has an area ratio of 2.0. The diameter of the combustor for this flight Mach number and compression level was $D_{comb} = 0.026$ m. Flow entered the isolator at Mach 2.56 and decelerates slowly due to wall friction. Fuel injection led to an instantaneous change in the 1-D properties, after which the combustion started to occur. Combustion along the expanding duct led to a drop in Mach number, an increase in temperature, and a smoothly varying pressure in response to the competing effects of combustion heat release and area increase. The peak pressure and temperature in the duct were $P/P_2 = 2.57$ and $T/T_2 = 1.94$, and the minimum Mach number was M = 1.32. The analysis supplied the 1-D properties exiting the combustor to the nozzle expansion model.
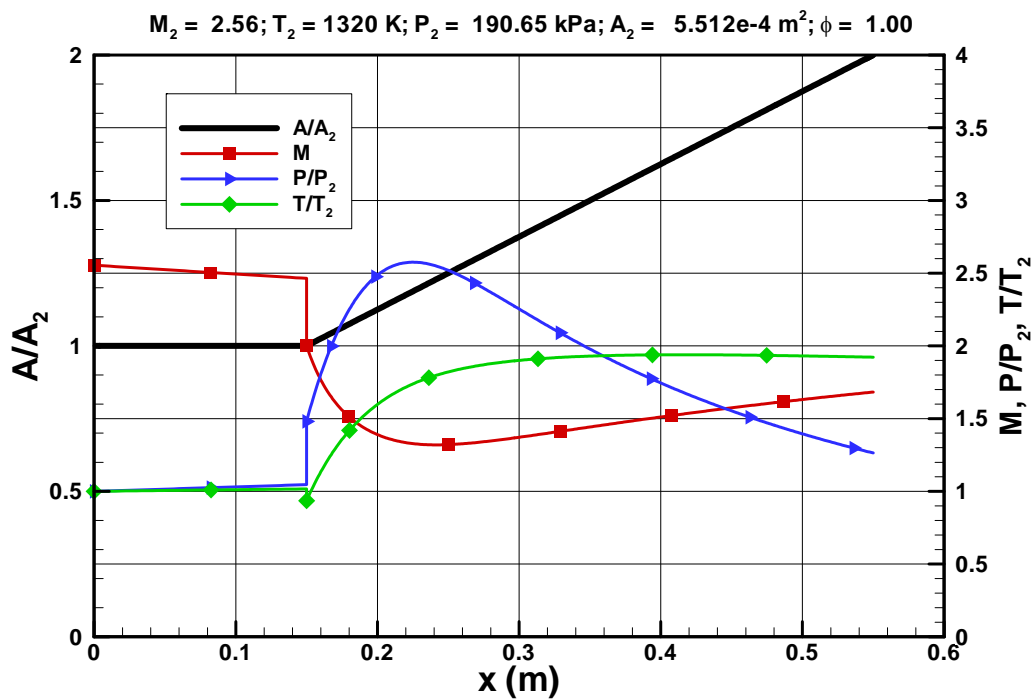

Figure 12: Example results of the combustor analysis.

Nozzle Expansion Model

The nozzle expansion was assumed to be defined by a fixed exit area ratio of $A_{10}/A_0 = 1.5$ which was different for each flight Mach number. This typically resulted in significant under-expansion ($P_{10} > P_0$) for all flight conditions. Losses in a scramjet nozzle are due to non-equilibrium chemistry (nozzle freezing), flow angularity and viscous effects. These were modelled here by the use of a nozzle efficiency, η_n, which was applied as a gross thrust coefficient as follows:

1) Given the conditions at station 4, expand the flow isentropically assuming chemical equilibrium from A_4 to A_{10} to obtain $F_{10,isentropic}$.

2) Apply the nozzle efficiency to the ideal stream thrust increment between stations 4 and 10; i.e. $F_{10} = F_4 + \eta_n [F_{10,isentropic} - F_4]$.

3) Assuming no heat loss in the nozzle, calculate the remaining flow properties at station 10 consistent with F_{10}.

A value of $\eta_n = 0.9$ was used in the study.

The results of the cycle calculations performed for this study are plotted in Fig. 13 in terms of the engine overall efficiency. At each flight Mach number there was a ψ that supplied an optimum η_o. This varied between $\psi = 4$-5, suggesting that classical thermodynamic analyses that indicate scramjet cycle efficiency increases continuously with inlet compression level are not applicable in this case. This may be due to the use of a divergent scramjet combustor wit han area ratio of two. This result, however, is a good one for inlet designers, as the higher the inlet compression level the more difficult it becomes to design an operational inlet.
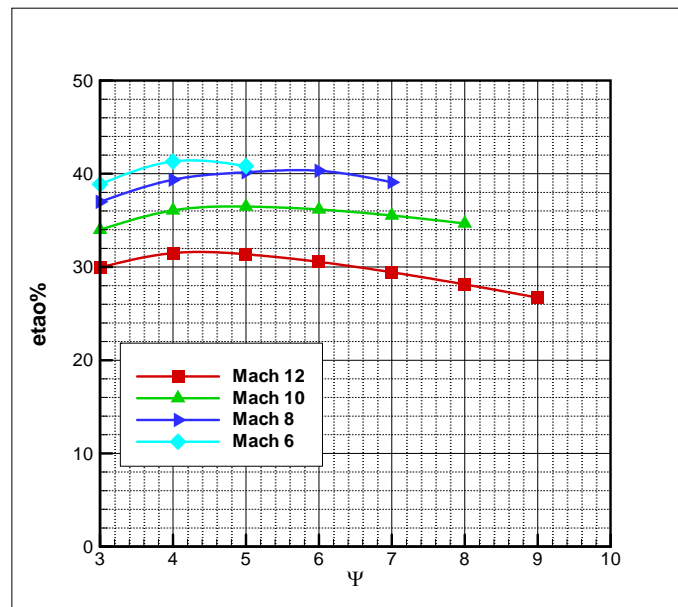

Figure 13: Overall scramjet cycle efficiency.

3.2   Non-Equilibrium Nozzle Effects

While it was shown in the last section that there is an optimum inlet compression level to produce maximum cycle efficiency, the analysis used to derive this result made use of equilibrium gas properties. This assumption is reasonable for calculating scramjet performance, except when the temperature of the flow entering the nozzle is too high. As inlet compression increases, the temperature of the flow entering the combustor rises. Combustion of fuel and air raises the temperature considerably higher, such that at the start of the nozzle, some portion of the oxygen and nitrogen in the air may be dissociated, and furthermore, some portion of the combustion product (H_2O in the case of hydrogen-air combustion) remains unformed. In the rapidly expanding nozzle process, recombination of the air and steam does not have time to fully occur, and a portion of the energy available from combustion is not realized.

Figure 14 shows a plot of the temperature at the combustor exit (T_4) for all conditions calculate in section 3.1. For the 3 flight Mach numbers where the engine was fuelled at an equivalence ratio of 1.0 (Mach 8, 10 and 12), flight Mach number (and therefore total enthalpy) did not have a large effect on T_4. The main factor that determined T_4 was ψ, which for example led to an increase in T_4 for Mach 10 flight from 2400 to 2700K for variation of ψ from 3 to 8. Mole fractions of N_2, O_2 and H_2O at the combustor exit are shown in Fig. 15 for Mach 8, 10 and 12. For clarity, the species mole fractions are normalized by their values if no dissociation has occurred and if the combustion reaction was fully completed. It is interesting to note that there was not a great deal of dissociation of N_2 and O_2. The main phenomenon which did show dependence on compression level was the percentage of H_2O present. This reduced from 90.4% for $\psi = 3$ to 79.7% for $\psi = 9$ for the Mach 12 case, and from 95.5% for $\psi = 3$ to 94.0% for $\psi = 8$ for Mach 8. For the worst case of frozen flow in the nozzle, these calculations would indicate that up to 10.7% of the energy of combustion would not be realized at high compression level. Fortunately the percentage of H_2O present at the optimum compression level indicated by the equilibrium analysis of section 3.1 ($\psi = 4$-5) indicated that non-equilibrium effects in the nozzle should not be too detrimental.
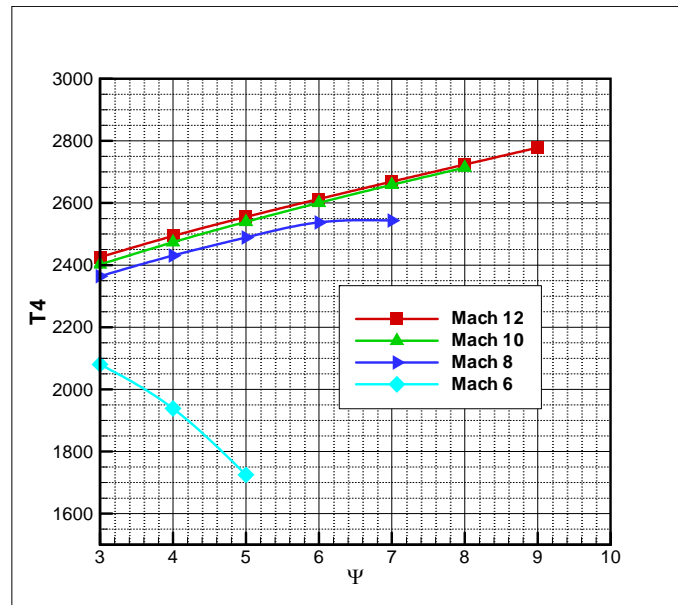

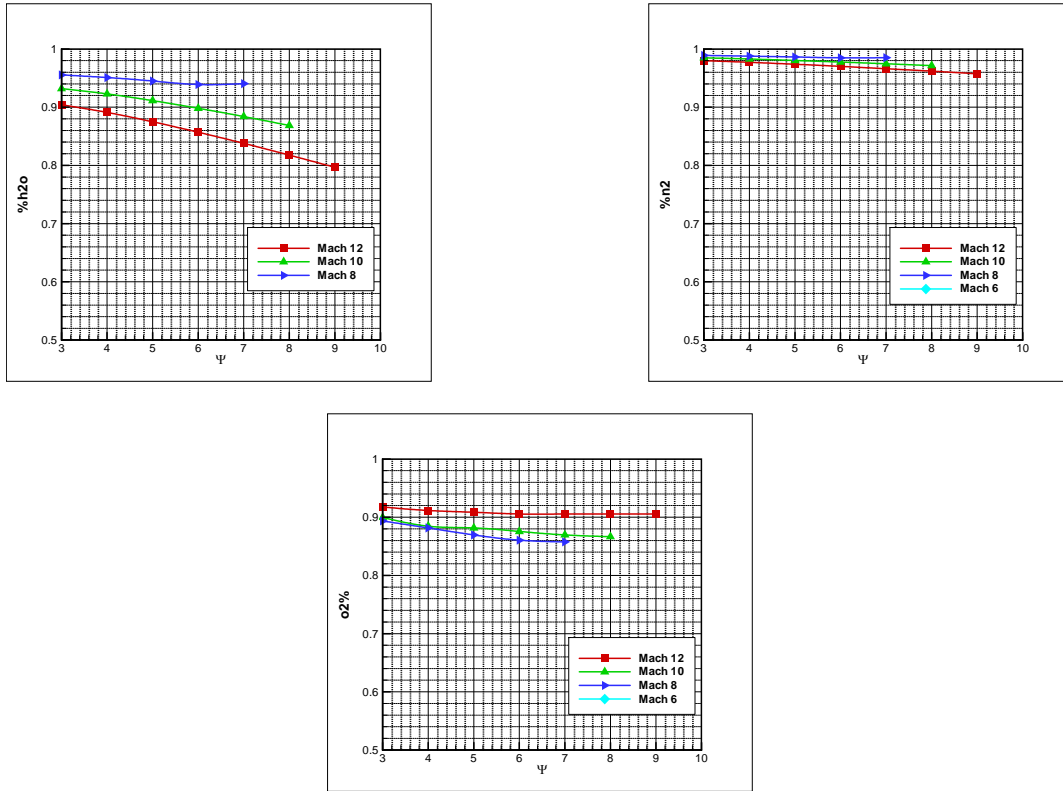**Figure 14: Static temperature at the entrance to the nozzle.**

Figure 15: Species mole fractions at the entrance to the nozzle.

3.3   Robust Combustion Requirements

Due to the high velocity of the air flow through a scramjet, the combustion processes must be rapid in order to be completed before the air exits the engine. To determine the limitations that this places upon combustor design, combustion modelling is typically separated into an initial time for ignition, and a further time for the combustion reaction to be completed. A corresponding length can be calculated for these processes (using a representative flow velocity), and these lengths (along with the mixing requirements) supply design criteria for scramjet combustor geometry. As the drag and heat load of the combustor have been found to be important parameters for overall scramjet system design, combustors should be as short as possible. Ignition and reaction times for H2/Air combustion can be estimated using the correlations of Pergament[16]. Given a representative combustor velocity of 2400 m/s and a local equivalence ratio between 0.2 and 2.0, the length required for ignition and reaction were calculated for a range of static temperatures and pressures as shown in Fig. 16. As can be seen, ignition length depends mainly on temperature, while reaction length depends strongly on both temperature and pressure. Representative values of ignition and reaction length are shown in Fig. 16 for a temperature of 1200K and pressures of 50 and 100 kPa.
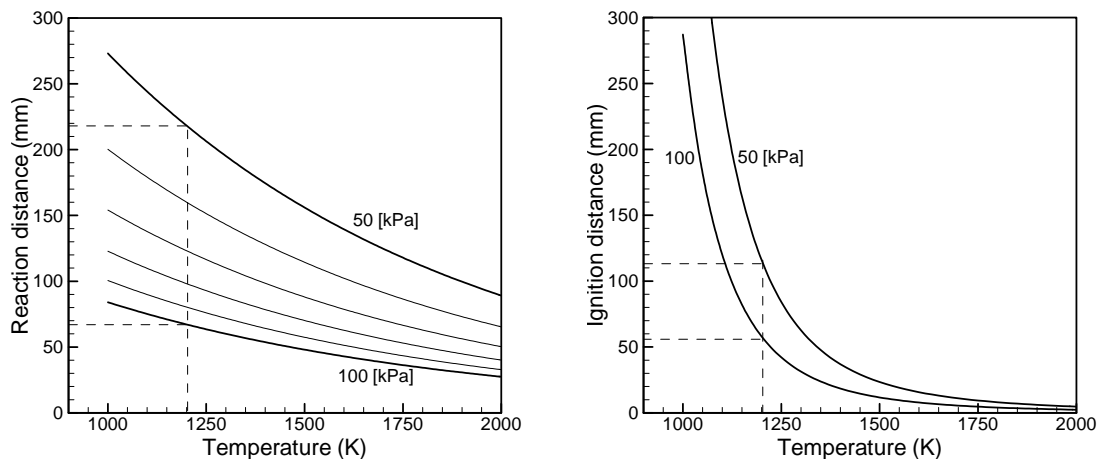
Figure 16: Ignition and reaction lengths of hydrogen assuming a combustor velocity of 2400 m/s.

Through the design of many scramjet systems it has been found that a successful solution to combustor design can be found by dealing with ignition and reaction separately. Short H2/Air ignition length requires temperatures well above 1000K, while lower temperatures are acceptable to complete the reaction, as long as a minimum pressure exists (typically ~ 50 kPa). This has led to flowpath designs that utilise an ignitor system to locally create the temperatures required for ignition (steps, cavities, spark plugs), but have an overall inlet compression level dictated by the need for a pressure high enough to complete the combustion reaction. In terms of the inlet design, therefore, the important requirement is simply the need to supply a minimum static pressure at the exit of the inlet. This pressure level is dictated by the combustor length available to complete the combustion reaction.

3.4   Operability limits

In the design of hypersonic inlets there are some key operability issues that must be addressed in order to arrive at a useful configuration. These are:

1) Inlet starting limits.

2) Boundary layer separation limits.

3) Minimization of external drag.

4) Performance at off-design Mach number.

The process of establishing supersonic flow through the inlet, known as inlet starting, puts a significant constraint on the internal contraction ratio of hypersonic inlets. This can be overcome through variable geometry, however, the weight and complexity of such can significantly degrade the overall system performance of a scramjet engine. Figure 17 shows a plot of some experimental data on the self-starting internal contraction ratio limit of 2-D and 3-D inlet configurations, as well as a theoretical starting limit developed by Kantrowitz & Donaldson[17]. The key parameter for inlet self-starting is the Mach number at the plane of cowl closure, M_c. It can be seen from the experimental data in Fig. 17 that the starting limit of Kantrowitz & Donaldson is relatively accurate for 2-D inlet geometries, but is conservative for the 3-D inlets shown. In general, the self-starting limits of particular inlet classes are determined through experimental testing, and become more restrictive as M_c decreases.
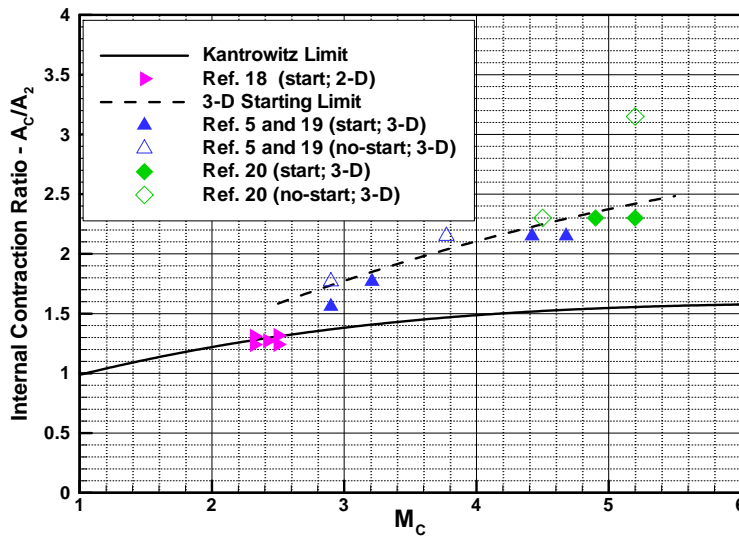
Figure 17: Experimental data on starting limits for 2-D and 3-D inlet geometries.

The desire for scramjet inlets to self-start, or need a minimum variable geometry to start, is a strong one when making choices about scramjet configurations for particular applications. This operability constraint leads to the desire for doing as little compression as possible. It is rare for the amount of internal contraction allowed by the self-starting limits to be enough on its own, so a mixed compression inlet is the most common. Inlet design issues related to starting remain a dominating constraint of all scramjet engine designs.

The flow through any practical hypersonic inlet will be turbulent, and can be prone to boundary layer separation due to shock interactions. While minor separation may be acceptable, large-scale boundary layer separation can create blockage of the engine and inlet unstart. Inlet flows are therefore required to satisfy established boundary layer separation limits[21].

Shock boundary layer interactions are generally separated into two categories:

1) Two-dimensional interactions such that those that occur at an unswept compression ramp or when a planar oblique shock reflects at a surface.

2) Swept interactions, such as the interaction produced by a planar oblique shock wave as it sweeps across a flat plate from a perpendicular fin.

For two-dimensional interactions, the pressure rise for incipient separation increases rapidly with Mach number. The following formulas are in general use:

$$P_{SEP}/P = 1.0 + 0.3M^2 \qquad M < 4.5$$

$$P_{SEP}/P = 0.17M^{2.5} \qquad M > 4.5$$

Conversely, incipient separation of swept interactions is independent of freestream Mach number and occurs at a pressure ratio of $P_{SEP}/P \sim 1.5$.

The minimization of external drag is an important aspect of the inlet design process. The external drag on the inlet will always be an important parameter when comparing the performance of different engine configurations, and the minimization of inlet external drag is one of the main drivers for airframe integration of scramjet engines. It also means that inlets with only external compression are not practical.

Finally, most inlet design methods are based on a particular design Mach number, usually at the upper limit of the operational Mach number range. Adequate off-design performance; i.e. at Mach numbers lower than the design point, is required, otherwise the vehicle may never reach its design point. This is particularly important for scramjet engines that must accelerate over a large Mach range.

3.5   Recommendation on Compression Level

The preceding sections described analysis of the key factors that affect the choice of inlet compression level in a hydrogen fuelled scramjet. Contrary to other references[3], overall cycle efficiency was not found to be strongly dependent on compression level. Whereas non-equilibrium effects in the nozzle and inlet operability constraints such as flowpath starting and boundary layer separation suggested a desire for a low compression level. The lower limit on compression level was supplied by the combustor pressure needed to complete the combustion reaction in a suitable length scale. So the recommendation of this study is to operate a scramjet with the lowest compression level that enables this to occur.

4.0   EXAMPLE INLET DESIGN: 3-D MACH 6-12 SCRAMJET FOR ACCESS-TO-SPACE APPLICATIONS

The history of scramjet development has seen a progression from experiments to validate the existence of supersonic combustion, to simple axi-symmetric configurations that owed their "pod-type" shape to gas turbine heritage, and then to airframe integrated engines with 2-D inlets and rectangular combustors (such as Hyper-X). In recent times it has become clear that from an overall system perspective, a flowpath based on 2-D geometry may not be optimum for high thrust/weight or robust fluid-dynamic performance of the engine. Scramjet flowpaths with elliptical or round combustors have therefore been studied[22,23]. These engine concepts attempt to take advantage of:

1) The inherent structural efficiency of rounded shapes. This potentially enables reduced structural weight.

2) The reduced wetted area of elliptical cross-sections relative to rectangular shapes for the same cross-sectional or flow area. (Reduced wetted area lowers viscous drag and cooling requirements in the high dynamic pressure combustor environment.)

3) The removal of the potentially detrimental fluid dynamic effects of corner flows in scramjet isolators and combustors. This may improve the back-pressure limits of the inlet/isolator, or alternatively, reduce isolator length requirements.

A key enabling technology for the use of elliptical combustors in airframe-integrated scramjets is the design of hypersonic inlets with 3-D shape transition. For vehicles with essentially planar forebody shapes, the required transition is from a rectangular-like capture area to an elliptical isolator/combustor shape (noting that a circle is an ellipse with an aspect ratio of unity). A design process developed for these Rectangular-to-Elliptical Shape Transition (REST) inlets[24] utilizes a quasi-streamline-tracing technique to produce an inlet with highly swept leading edges, a cut back cowl, and the desired shape transition to an elliptical throat. The REST inlets resulting from these procedures have almost 100% mass capture at the design Mach number, and operate below the design Mach number by spilling air past the cut back cowl. An important aspect of this computationally intensive design procedure is the ability to reduce inlet length until shock wave/boundary layer separation criteria are met.

A three-dimensional scramjet for access-to-space applications has recently undergone testing in the T4 shock tunnel at The University of Queensland[25]. This flowpath is a REST configuration with a design flight envelope from Mach 6-12, and is a candidate engine for the airbreathing portion of a three-stage rocket-scramjet-rocket access-to-space system[26]. At the Mach 12 design point the RESTM12 engine operates as a pure scramjet, however in order to be effective at the lower end of its flight envelope, allowances have been made for dual-mode operation below Mach 7. A dimensioned schematic of the engine is shown in Fig. 18. The overall model was 1.98 m long and consisted of a forebody plate, REST inlet, elliptical combustor, and a short elliptical nozzle with a final area ratio of 8.0 relative to the inlet throat. The design of the inlet for this flowpath was a challenging problem, the details of which are described in the next section.
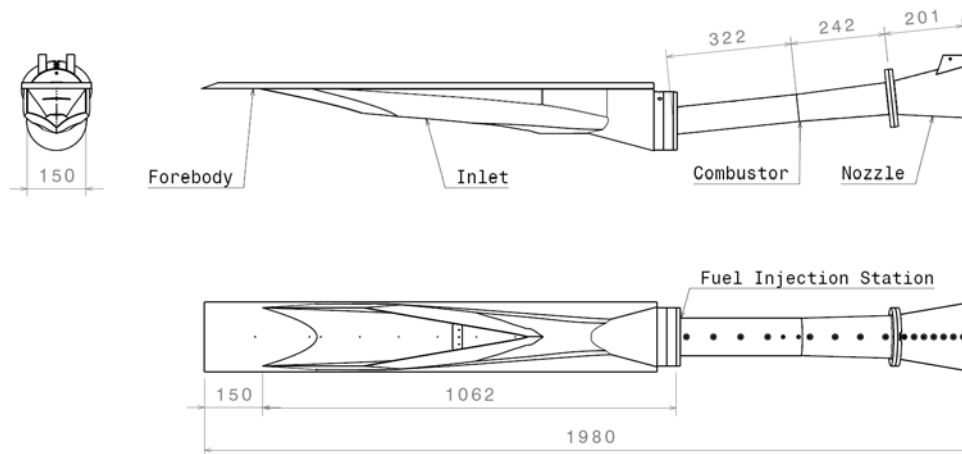

Figure 18: Schematic of the RESTM12 engine model (dimensions in mm).

4.1   REST Inlet Design for Mach 6-12

The inlet geometry for the RESTM12 engine was generated using the 3-D inlet design tools of Ref. 7. This method combined a quasi-streamlinetraced inviscid technique with a correction for three-dimensional boundary layer growth, to design an inlet with nearly rectangular capture and a smooth transition to an elliptical throat. These techniques were applied with a design flight Mach number of 12, assuming the engine was installed on a vehicle with a forebody equivalent to a 6 degree wedge. So the Mach number of the flow entering the inlet was $M_1 = 9.113$. The required inlet compression ratio was determined by the assumption of a flight dynamic pressure of $q_0 = 50$ kPa and the requirement of a combustor entrance pressure high enough for completion of H_2-Air combustion in the available length; in this case $P_2 = 50$ kPa. This corresponded to an overall compression ratio of $P_2/P_0 = 100.8$, and an inlet compression ratio $P_1/P_0 = 22.25$. The resulting inlet has a geometric contraction ratio of CR = 6.61, and an internal contraction ratio of CRI = 2.26. Inlets of this class have been shown in experiments to self-start at CRI values significantly higher than the Kantrowitz limit (Fig. 17). Based on these experiments, the lower limit for self-starting of the RESTM12 inlet was estimated to be $M_1 \sim 5.0$.

While the inlet design process was conducted at the maximum operational Mach number of the engine, its capability, mass capture and efficiency were determined over the full operational range using CFD. These CFD solutions were calculated with the NASA Langley code VULCAN[27] on a 2 million cell grid using wall functions to model boundary layer phenomenon. A thermally perfect model was used for the air and flow was assumed to be turbulent from the forebody leading edge. Figure 19 shows the symmetry plane Mach number contours for the inlet when the vehicle is flying at $M_0 = 10$, and $q_0 = 50$ kPa, corresponding to $M_1 = 7.950$. Note that the highly notched cowl allows flow spillage when M_1 is below the design point

for the inlet ($M_1 = 9.113$). The flow properties at the exit of the inlet were calculated using flux conserving methods. At this condition the flow pressure and temperature exiting the inlet were $P_2 = 54.64$ kPa and $T_2 = 1000.$ K.

Figure 19: Symmetry plane Mach number contours in the RESTM12 inlet at $M_0 = 10$.

Figure 20 shows the variation of the important inlet/forebody performance parameters over the full operational range. The inlet has full capture at its Mach 12 design point, dropping to $m_c = 0.81$ at Mach 6. The overall pressure ratio at Mach 12 was slightly above the requirement of $P_2/P_0 = 100.8$, and this pressure ratio reduced steadily to 39.4 at Mach 6. Despite this large drop in pressure ratio, the flow pressure leaving the inlet at Mach 6 was $P_2 = 78.2$ kPa. Interestingly, the efficiency of the inlet remained high over the full Mach range with η_{KE_AD} varying between 0.97 and 0.98.
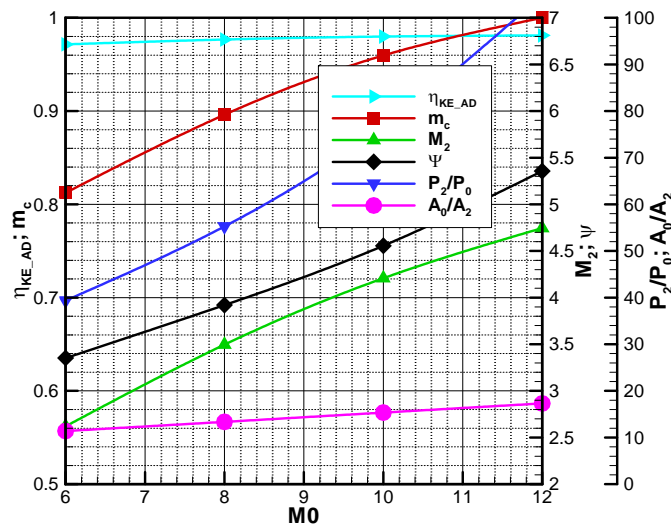

Figure 20: RESTM12 Inlet capability parameters.

5.0   CONCLUDING REMARKS

The inlet configuration chosen for a scramjet is a dominating feature of the entire configuration. The choice of inlet type is strongly dependent on the requirements for the engine, particularly the Mach number range of operation the proposed flight trajectory. It was also shown that the compression level of a

scramjet inlet should be set by the minimum combustor pressure that allows completion of the combustion reaction in a length scale suitable for the application. Recent research indicates that three-dimensional configurations show considerable promise.

6.0 REFERENCES

[1] Ferri, A., 1964, "Review of the problems in application of supersonic combustion", Journal of the Aeronautical Society, 64(645), p575-597.

[2] Van Wie, D. M., 2001, "Scramjet Inlets", Scramjet Propulsion, Progress in Astronautics and Aeronautics, AIAA Washington DC, Chapter 7.

[3] Heiser, W.H. and Pratt, D.T., 1994, "Hypersonic Airbreathing Propulsion", AIAA Education Series.

[4] Waltrup. P.J., Billg, F.S. and Stockbridge, R.D., 1982, "Engine sizing and integration requirements for hypersonic airbreathing missile applications", AGARD-CP-207, No. 8.

[5] Smart, M.K., 2001, "Experimental Testing of a Hypersonic Inlet with Rectangular-to-Elliptical Shape Transition", Journal of Propulsion and Power, Vol. 17, No. 2, pp 276-283.

[6] Molder, S., 1999, "Performance of three hypersonic inlets", paper 1430, 22nd International Symposium on Shock Waves, London, UK.

[7] Van Wie, D.M. and Ault, D.A., "Internal flowfield characteristics of a two-dimensional inlet at Mach 10", Journal of Propulsion and Power, Vol. 12, No. 1, 1996, pp 158-164.

[8] Andrews, E.H. and Mackley, E.A., 1976, "Analysis of experimental results of the inlet for the NASA hypersonic research engine aerothermodynamic integration model", NASA TM X-3365.

[9] Trexler, C.A. and Souders, S. W., 1975, "Design and performance at a Mach number of 6 of an inlet for an integrated scramjet concept", NASA TN D-7944.

[10] Billg, F.S., 1995, "Supersonic combustion ramjet missile", Journal of Propulsion and Power, 11(6), p1139-1146.

[11] Waltrup, P.J., 1990, "The dual combustor ramjet: a versatile propulsion system for hypersonic tactical missile applications", AGARD CP-527, No. 7.

[12] McClinton, C.R., 2006, "X-43 – scramjet power breaks the hypersonic barrier: Dryden lectureship in research for 2006", AIAA paper 2006-1.

[13] Curran and Craig.

[14] Smart, M. K., "Scramjets," *Aeronautical Journal*, Vol. 111, No. 1124, 2007, pp. 605-619.

[15] Ortwerth, P.J., 2001, "Scramjet Vehicle Integration", Scramjet Propulsion, Progress in Astronautics and Aeronautics, AIAA Washington DC, Chapter 17.

[16] Pergamnet, H. S., "Theroretical analysis of non-equilibrium hydrogen-air ractions in flow systems," *AIAA-ASME Hypersonic Ramjet Conference*, No. 63113, 1963.

[17] Kantrowitz, A., and Donaldson, C., 1945, "Preliminary Investigation of Supersonic Diffusers," NACA WRL-713.

[18] Van Wie, D.M., Kwok, F.T. and Walsh, R.F., "Starting characteristics of supersonic inlets", AIAA Paper 96-2914, July 1996.

[19] Smart, M.K. and Trexler, C.A., "Mach 4 Performance of a Fixed-Geometry Hypersonic Inlet with Rectangular-to-Elliptical Shape Transition", Journal of Propulsion and Power, Vol. 20, No. 2, pp 288-293, 2004.

[20] Hartill, W.B., "Analytical and experimental investigation of a scramjet inlet of quadriform shape", US Air Force, TR AFAPL-TR-65-74, Marquardt Corp. August 1965.

[21] Korkegi, R.H., 1975, "Comparison of shock induced two- and three-dimensional incipient turbulent separation", AIAA Journal 13(4), p534-535.

[22] Smart, M.K. and Ruf, E.G., 2006, "Free-jet Testing of a REST Scramjet at Off-Design Conditions", AIAA paper 2006-2955.

[23] Beckel, S.A., Garrett, J.L. and Gettinger, C.G., 2006, "Technologies for Robust and Affordable Scramjet Propulsion", AIAA paper 2006-7980.

[24] Smart, M.K., 1999, "Design of Three-Dimensional Hypersonic Inlets with Rectangular-to-Elliptical Shape Transition", Journal of Propulsion and Power, Vol. 15, No. 3, pp 408-416.

[25] Suraweera, M. V. and Smart, M. K. Shock Tunnel Experiments with a Mach 12 Rectangular-to-Elliptical-Shape-Transition Scramjet at Offdesign Conditions. *Journal of Propulsion and Power* **2009,** *25* (3), 555-564.

[26] Smart, M. K. and Tetlow, M. R. Orbital Delivery of Small Payloads using Hypersonic Airbreathing Propulsion. *Journal of Spacecraft and Rockets* **2009,** *46* (1), 117-125.

[27] White, J. A., and Baurle, R. A., "Viscous Upwind aLgorithm for Complex flow ANalysis, User manual," NASA Langley Research center, Langley Virginia, release version 6.0.